

# Rotating Ferrofluid Drops

Andreas Engel, Alexander V. Lebedev<sup>a</sup>, and Konstantin I. Morozov<sup>a</sup>

Institut für Physik/Statistische Physik, Carl-von-Ossietzky-Universität, D-26111 Oldenburg

<sup>a</sup> Institute of Continuous Media Mechanics, 1 Korolev Street, 614013 Perm, Russia

Reprint requests to A. E.; E-mail: engel@theorie.physik.uni-oldenburg.de

Z. Naturforsch. **58a**, 703 – 721 (2003); received September 30, 2003

We study the stationary shapes and the rotational motion of drops of magnetic fluids floating in a non-magnetic liquid of equal density and spun up by an externally applied rotating magnetic field. For a sufficiently large magnetic susceptibility of the drop fluid transitions to non axial-symmetric shapes take place when the field amplitude is increased. We give a detailed theoretical account of the character of these shape bifurcations, of the resulting stationary drop forms, and of the slow rotational motion of the drop and compare our findings with results obtained in an experimental realization of the system. Quantitative agreement between theory and experiment can be obtained when saturation effects in the magnetization curve of the ferrofluid are taken into account.

PACS numbers: 47.20.Hw, 47.55.Dz, 75.50.Mm

*Key words:* Hydrodynamic Stability; Equilibrium Shapes; Magnetic Fluids.

## 1. Introduction

The equilibrium shapes of rotating fluid bodies are of interest in various fields of physics. The most prominent classical contexts are the stationary forms of heavenly bodies [1] and the geometry of atomic nuclei in nuclear fission [2]. More recent examples include rotating non-neutral plasmas, lasers cooled in a Penning trap [3], and tank-treading elliptical membranes in a shear flow which are used as model for the motion of human red blood cells [4].

The investigation of stationary shapes of rotating bodies in laboratory experiments usually employs fluid drops immersed in another, immiscible liquid of the same density. These drops can be spun up by using a rotating shaft [5] or applying an acoustic torque [6]. For drops made from polarizable fluids it is convenient to use rotating electric [3] or magnetic fields [7–9] to set the drop into rotation.

In the present paper we investigate rotating *ferrofluid* drops theoretically and experimentally. Ferrofluids are suspensions of ferromagnetic nanoparticles in suitable carrier liquids combining the hydrodynamic behaviour of Newtonian liquids with the magnetic properties of super-paramagnets [10]. Many of their fascinating properties stem from the interaction between hydrodynamic and magnetic degrees of freedom. A rotating external magnetic field induces

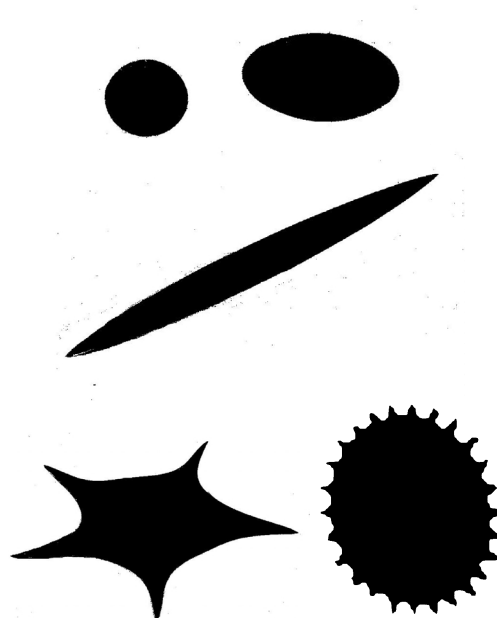


Fig. 1. Top view of some drop shapes as observed in the experiment for increasing magnetic field strength. For large fields the axis-symmetric shape of the drops is impaired by peaks at the periphery, resulting from the normal field instability.

a rotation of the nano-particles which in turn, due to their viscous coupling to the surrounding liquid, trans-

fer the angular momentum to the whole drop. We will study the stationary *shape* of the drop and in particular possible bifurcations to *non axis-symmetric* configurations as well as the *rotation* of the drop together with the hydrodynamic flow fields in the drop and in the surrounding liquid. In Fig. 1 some experimentally observed drop shapes are displayed. Note that the photos are taken along the symmetry axis of the rotating field.

Part of our results was published in the short communication [9]. In the present manuscript we give a substantially enlarged and comprehensive analysis of the problem. The case of an *elliptically* polarized magnetic field is treated in [11] where also movies of the experiments are to be found.

In a *static* magnetic field a floating ferrofluid drop is known to elongate along the field direction [12] with a shape very well described by a prolate ellipsoid of revolution. If the field rotates slowly enough so as to allow the drop to adapt its shape to the moving field direction the drop shape remains elongated and the whole drop follows the field rotation with a certain phase lag [13–15]. On the other hand, in a magnetic field rotating with a frequency much higher than the inverse relaxation time of the drop shape the drop cannot follow the field and is *smearred* in the plane of the rotating field. Its shape is then well approximated by an *oblate* spheroid. It is this regime of *high* frequency of the field rotation which we will study.

The behaviour of magnetic drops under the influence of a fast rotating magnetic field was first investigated systematically in the pioneering work of Bacri *et al.* [7]. It was found that for both small and large magnetic fields the equilibrium shape of the drop is an oblate spheroid where in the latter case peaks at the periphery due to the normal field instability [10, 16] give rise to a “spiny starfish” form. For intermediate values of the magnetic field strength various transient non axis-symmetric shapes like “worms” and “loops” were found. In later experiments [17] even more exotic forms of “S”-, “O”-, and “8”-shapes were reported. On the theoretical side (see also [18]) it was noted that for intermediate values of the magnetic field the axis-symmetric state may become unstable if the susceptibility of the ferrofluid exceeds  $\chi \simeq 0.56$ . Hence for increasing field strength the bifurcation scenario axis-symmetric spheroid to non axis-symmetric form and back to axis-symmetric spheroid was suggested, which agrees qualitatively with the experiments. Due to the special preparation techniques

used to synthesize the magnetic fluid, however, the experiments in [7] were characterized by quite unusual parameters. The drops were rather small with a typical radius  $R \simeq 10 \mu\text{m}$ , the magnetic susceptibility was very high,  $\chi \simeq 3 \dots 5.5$ , the interface tension between the ferrofluid and the surrounding liquid was extremely small,  $\alpha \simeq 10^{-3} \text{ dyn/cm}$ , and the viscosity of the ferrofluid was very high,  $\eta \sim 1 \text{ P}$ , exceeding the viscosity of the surrounding fluid by two orders of magnitude. These parameters give rise to very elongated and *instationary* shapes at intermediate field values which made a detailed comparison between theory and experiment in this regime impossible.

In contrast, our experiments are characterized by rather different parameters. We use large drops with  $R \simeq 2 \dots 5 \text{ mm}$  of ferrofluids with moderate values of the susceptibility,  $\chi \simeq 0.3 \dots 2$ . The interface tension is about  $3 \text{ dyn/cm}$  as for usual liquids, and the viscosities of the ferrofluid and of the surrounding liquid are comparable. As a consequence we find at intermediate values of the magnetic field strength well-defined transitions to *stationary* non axis-symmetric shapes which can often be well approximated as *three-axes* ellipsoids. After a detailed theoretical study of these shape transitions we find *quantitative* agreement with our experimental results if we take into account magnetic saturation effects in the ferrofluid. Due to the relative equality of the viscosities inside and outside the drop, a theoretical investigation of the drop rotation is inevitably linked with the determination of the hydrodynamic flow fields in both fluids. Building on the classical results of Jeffrey [19] we analyze the rotational motion of the drop theoretically and obtain again good agreement with the experiment.

The paper is organized as follows. In Sect. 2 we present our basic strategy to attack the problem theoretically and introduce the main approximations made. Sections 3 and 4 contain the discussion of the shape and the rotation problem, respectively. In each of these sections we first consider the general approach, followed by the analysis for a linear magnetization law of the ferrofluid. At the end we discuss the influence of saturation effects in the ferrofluid magnetization. Section 5 is devoted to the description of the experiments. Finally section 6 contains some conclusions. In the appendix we derive a relation between the energy dissipation balance in the system and the continuity of the average tangential stress at the drop surface, which is important for our approach to the rotation problem.

## 2. Preliminary Remarks

We consider a drop of a ferrofluid floating in an immiscible liquid of equal density and under the influence of an external magnetic field  $\mathbf{G}$  which in the absence of the drop is spatially homogeneous and rotating in the horizontal  $x$ - $y$ -plane with constant angular frequency  $\omega$ . The main impact of the magnetic field on the drop is to deform its shape and to set it into rotation with a frequency  $\Omega$ . We will only discuss the situation in which the field frequency  $\omega$  is significantly smaller than the inverse Brownian relaxation time of the ferrofluid,  $\omega\tau_B \ll 1$ , but at the same time much larger than the rotation frequency  $\Omega$  of the drop,  $\Omega \ll \omega$ . The values characterizing our experiments are  $\tau_B \lesssim 10^{-4}$  s,  $\omega \simeq 3 \cdot 10^3$  s $^{-1}$ , and  $\Omega \lesssim 1$  s $^{-1}$ . The complementary case of a slowly rotating field,  $\Omega \simeq \omega$ , is discussed in [14].

Due to the magnetic polarizability of the ferrofluid the magnetic field gives rise to volume and surface forces which are described by the magnetic stress tensor

$$\sigma_{ik}^m = \frac{1}{4\pi} \left( H_i B_k - \frac{1}{2} H^2 \delta_{ik} \right) + \frac{1}{2} (M_i H_k - M_k H_i), \quad (1)$$

where  $\mathbf{B}$ ,  $\mathbf{H}$  and  $\mathbf{M}$  denote the magnetic induction, the magnetic field (both in the presence of the magnetic fluid) and the magnetization, respectively. The first term is the usual Maxwell stress tensor, the second one is the augmentation due to Shliomis to describe non-equilibrium situations [20]. As we will see below, the *rotation* of the drop is a direct consequence of magneto-dissipative effects, and the additional term in the stress tensor is crucial.

The magnetic volume force density  $\mathbf{f}^m$  corresponding to (1) has the well-known form

$$\mathbf{f}^m = (\mathbf{M} \cdot \nabla) \mathbf{H} + \frac{1}{2} \nabla \times (\mathbf{M} \times \mathbf{H}). \quad (2)$$

To solve the described problem in full generality is a formidable theoretical task, analytically as well as numerically. One had to simultaneously solve the hydrodynamic equations for the two liquids including the magnetic force densities for the ferrofluid, and the magneto-static Maxwell equations for the magnetic fields  $\mathbf{B}$  and  $\mathbf{H}$ . Both sets of equations have to obey boundary conditions at the *free surface* of the drop the determination of which is part of the problem.

As first and decisive steps of our analysis we hence propose some approximations which on the one hand describe the experimental situation to sufficient accuracy and on the other hand render the theoretical problem tractable. Our main simplifying assumptions are:

- i) The shape of the drop is approximated by a three-axes ellipsoid.
- ii) The shape is assumed to be determined solely by the balance between the surface energy and the magnetic energy.
- iii) The hydrodynamic flow problem will be treated within the Stokes approximation.
- iv) The flow inside the drop is horizontal and of uniform vorticity.

The first assumption describes the experimental situation rather well except for those values of the magnetic field for which large peaks develop at the periphery of the drop (cf. Fig. 1 and Sect. 5). On the other hand it simplifies the analysis considerably. Firstly, within this approximation the shape of the drop is uniquely described by the values of the three semi-axes  $a \geq b \geq c$ . Because the volume of the drop is conserved, in fact *two* parameters are sufficient which we choose to be the semi-axes *ratios*  $\epsilon_b = a/b$  and  $\epsilon_c = a/c$ . Secondly, the assumption simplifies the calculation of the surface energy since for the surface area  $S$  of an ellipsoid there is an explicit formula available. Thirdly, the magneto-static problem of a magnetizable ellipsoid in a homogeneous external field can be solved explicitly [21]. Remarkably, the internal field  $\mathbf{H}$  and the magnetization  $\mathbf{M}$  are spatially *homogeneous*, and correspondingly the *bulk* force density (2) is *identically zero*.

Within the approximation of an ellipsoidal shape the whole impact of the magnetic field is hence via *surface* stresses at the drop boundary. Our second assumption above is substantiated by estimating the order of magnitudes of the different stresses relevant in our problem. The typical capillary normal stress is given by  $p_c \sim \alpha/R$  where  $\alpha$  denotes the interface tension and  $R$  the radius of the spherical drop. Our experiments are characterized by  $\alpha \simeq 5$  dyn/cm and  $R \simeq 0.5$  cm, hence we have  $p_c \simeq 10$  dyn/cm $^2$ . The magnetic normal stress is given by  $p_m \sim \pi M_n^2$ , where  $M_n$  is the normal component of the fluid magnetization [10]. For a spherical drop of magnetic susceptibility  $\chi$  in a magnetic field  $G$  we have  $M = 3\chi/(3 + 4\pi\chi) G$  [21]. Typical experimental values are  $\chi \simeq 0.72$  and  $G \simeq 20$  Oe, giving rise to  $p_m \simeq 10$  dyn/cm $^2$ . The viscous

stresses acting on the rotating drop can be estimated as  $p_v \sim \eta^{(e)}\Omega$ , where  $\eta^{(e)}$  denotes the dynamic viscosity of the surrounding fluid. With the experimental values  $\eta^{(e)} \simeq 0.5$  P and  $\Omega \lesssim 1$  s<sup>-1</sup> we get  $p_v \lesssim 1$  dyn/cm<sup>2</sup>. Consequently the capillary and magnetic stresses are comparable and exceed the viscous stress by at least one order of magnitude. For the determination of the *shape* of the drop the viscous stress is therefore negligible. The equilibrium between the two *normal* stresses due to capillarity and magnetization can be rewritten as extremum condition for the sum of the surface and magnetic energy. Averaging the latter over one period of the external field we arrive at a quasi-static problem which will serve as the starting point to determine the shape of the rotating drop as described in detail in Section 3. Notwithstanding its smallness, the viscous stresses will be important in the analysis of the *motion* of the drop to which the normal stresses do not contribute.

It is important to note that the above estimates were made for a *spherical* drop as it exists without magnetic field. When the magnetic field is switched on, the drop deforms and the values of the various stresses change. However, for the parameter values used in our experiments the viscous torques turn out to be irrelevant for the shape of the drop for *all* occurring values of the semi-axes ratios  $\epsilon_b$  and  $\epsilon_c$ . On the other hand, for the micro-drops studied in [7, 17] the viscous stresses become comparable to the magnetic and capillary ones for large elongations of the drops. The motion of the drop and the associated fluid flow then start to influence the drop shape. We believe this to be the main reason for the variety of *non-stationary* shapes observed in these experiments.

The third assumption made above is reasonable since the Reynolds number for our system can be estimated as  $\text{Re} \sim \rho\Omega R^2/\eta^{(e)}$ , and with  $\rho \lesssim 1.8$  g/cm<sup>3</sup> we find  $\text{Re} \lesssim 0.9$ . Accordingly the inertial term in the Navier-Stokes equation can be neglected. Since the magnetic force density is zero as a consequence of assumption i) the stationary flow fields  $\mathbf{v}^{(i)}$  and  $\mathbf{v}^{(e)}$  of the internal and external fluid, respectively, have to satisfy the simple equations

$$\eta^{(i,e)} \Delta \mathbf{v}^{(i,e)} = \nabla p^{(i,e)}, \quad (3)$$

where  $p^{(i)}$  and  $p^{(e)}$  denote the pressure inside and outside the drop, respectively. In fact, deriving these equations we have tacitly made two more approximations which deserve some discussion. First, by assuming  $\eta^{(i)}$

to be a constant we ignored the very small change of the viscosity of the ferrofluid due to the magnetic field, known as *rotational viscosity* [20]. This change is of order  $\Omega\tau_B$  which in our experimental situation, characterized by  $\Omega \ll \omega$  and  $\omega\tau_B \ll 1$ , is indeed very small. Second we neglected the heating of the ferrofluid due to its periodic re-magnetization. The radial temperature difference within a spherical drop induced by a periodic magnetic field can be estimated as [22]

$$\Delta T = \frac{3}{4} \frac{\chi_2 \omega G^2 R^2}{(3 + 4\pi\chi_1)^2 \vartheta}, \quad (4)$$

where  $\chi_2$  denotes the imaginary part of the ferrofluid susceptibility and  $\vartheta$  is the heat conductivity of the magnetic fluid. With the typical experimental data as given above, completed by  $\chi_2 \simeq 0.087$  and  $\vartheta = 2 \times 10^4$  erg/(cm s K), we find for the temperature difference the negligible value  $\Delta T \simeq 0.007$  K.

Finally, the last assumption states that due the small Reynolds number, i.e. the dominance of the viscous terms in the flow problem, the stationary internal flow field  $\mathbf{v}^{(i)}$  can be well approximated by the two-dimensional elliptical form

$$\mathbf{v}^{(i)} = \left( -\zeta y \frac{a}{b}, \zeta x \frac{b}{a}, 0 \right), \quad (5)$$

matching the shape of the drop. Here the parameter  $\zeta$ , related to the vorticity of the flow field, remains for the time being undetermined. Building on assumption iii) and the corresponding *linearity* of the hydrodynamic equations it is convenient to make for the external flow field the *superposition* ansatz

$$\mathbf{v}^{(e)} = \mathbf{v}^{(i)} + \mathbf{v}^{(J)}. \quad (6)$$

As will be discussed in detail in Section 4, the additional term  $\mathbf{v}^{(J)}$  describes the flow field of a viscous fluid surrounding a *rigid* ellipsoid, i.e. nothing but the well known Jeffrey solution of the Stokes equations [19]. Within the above approximations the solution of the hydrodynamic flow problem is hence reduced to the determination of the two parameters  $\Omega$  and  $\zeta$ .

To calculate both  $\Omega$  and  $\zeta$  we need two equations reflecting the *stationarity* of the drop rotation. As first one we use the *balance between* viscous and magnetic *torques* on the drop, which is obviously mandatory for a stationary rotation. The second one derives from the *energy dissipation balance*, stating that the inflow of

magnetic energy to the drop must be equal to the energy dissipation rate in the viscous flows of the internal and external fluids. In the appendix we show that this condition is equivalent to the requirement of continuity of tangential stresses when *integrated* over the complete drop surface of the form

$$\int_{\partial V} dS v_i^{(i)} \sigma_{ik}^{(i)} \nu_k = \int_{\partial V} dS v_i^{(e)} \sigma_{ik}^{(e)} \nu_k. \quad (7)$$

Here  $\sigma_{ik}^{(i)}$  and  $\sigma_{ik}^{(e)}$  denote the stress tensors inside and outside the drop respectively and  $\nu$  is the surface normal. Note that an exact solution of the problem would require a *point-wise* continuity of tangential stresses at the drop surface. Employing the approximation of an ellipsoidal shape and an internal flow of the form (5), however, this condition cannot be strictly fulfilled. Instead we replace it by an *average* continuity requirement related to the energy dissipation balance in the system.

To summarize this section, we have divided the original problem into *two subtasks*. In the first one the *shape* of the ferrofluid drop is determined by minimizing the sum of the surface energy and of the time averaged magnetic energy in the geometry parameters  $\epsilon_b$  and  $\epsilon_c$ . The contributions from the fluid flow are negligible for this subtask, and we hence assume the liquids to be at rest. Our method to solve the problem of the drop shape is hence a direct generalization of the energetic approach used for a *static* field in [12]. This approximation is quantitatively accurate since the rate of energy dissipation is very small. This refers both to the viscous dissipation, which is proportional to the slow rotation frequency  $\Omega$  of the drop, and to the magneto-dissipation, which is of the order  $(\chi_2/\chi_1)^2 \sim (\omega\tau_B)^2 \ll 1$ .

In the second subtask we determine the *rotation frequency* of the drop for a *given* shape parameterized by the results for  $\epsilon_b$  and  $\epsilon_c$  obtained in the first subtask. In the co-moving coordinate system, in which the drop shape is at rest, we use the ansatzes (5) and (6) for the flow fields of the internal and external fluids, respectively. Building on the classical solution of Jeffrey for the flow around a rotating rigid ellipsoid we determine the two parameters  $\Omega$  and  $\zeta$  of our ansatz from the balance of viscous and time averaged magnetic torques and from the integrated balance of tangential stresses at the drop surface.

The two subtasks are discussed in detail in Sect. 3 and 4, respectively. In both cases the frequency of the

external magnetic field is kept constant and the quantities of interest are studied with respect to their dependence on the field *amplitude*  $G$  characterized by the dimensionless magnetic bond number

$$B = \frac{G^2 R}{\alpha}. \quad (8)$$

### 3. The Shape of the Drop

#### 3.1. General Remarks

As explained in the last section we will determine the shape of the drop by minimizing the sum of surface energy and time averaged magnetic energy

$$E = \alpha S + \bar{E}_m. \quad (9)$$

Here  $S$  is the surface of the drop,  $\alpha$  the surface tension, and the overbar denotes a time average over one period of the applied magnetic field. The time dependent magnetic energy is given by [21]

$$E_m(t) = - \int_V d^3r \int_0^{G(t)} dG' \mathbf{M}(\mathbf{r}, \mathbf{G}'), \quad (10)$$

where the first integral is over the volume of the drop,  $\mathbf{G}$  denotes the external magnetic field in the absence of the drop and  $\mathbf{M}(\mathbf{r}, \mathbf{G})$  is the local magnetization of the ferrofluid. In our case  $\mathbf{G}$  is a spatially homogeneous rotating field of amplitude  $G$  with Cartesian coordinates

$$\mathbf{G} = (G \cos(\omega t), G \sin(\omega t), 0) = G \Re\{e^{i\omega t}(1, -i, 0)\}. \quad (11)$$

Since  $\Omega \ll \omega$  we will not distinguish between the frequency of the external field in the laboratory frame and in the co-moving coordinate system in which the drop is at rest.

A crucial assumption of our approach is the approximation of the drop shape by a three-axes ellipsoid with semi-axes  $a \geq b \geq c$ . This supplies us immediately with an explicit expression for the surface of the drop in terms of the ratios  $\epsilon_b = a/b$  and  $\epsilon_c = a/c$  between the semi-axes of the form

$$S = 2\pi R^2 \epsilon_b^{2/3} \epsilon_c^{-4/3} \times \left[ 1 + \frac{\epsilon_c}{\epsilon_b \sqrt{\epsilon_c^2 - 1}} (\mathcal{F}(m, \kappa) + (\epsilon_c^2 - 1)\mathcal{E}(m, \kappa)) \right]. \quad (12)$$

Here  $R = (abc)^{1/3}$  is the radius of the drop in the absence of the magnetic field and  $\mathcal{F}$  and  $\mathcal{E}$  are elliptic integrals of first and second kind, respectively [23]. Moreover

$$m = \frac{\sqrt{\epsilon_c^2 - 1}}{\epsilon_c} \quad \text{and} \quad \kappa = \sqrt{\frac{\epsilon_c^2 - \epsilon_b^2}{\epsilon_c^2 - 1}}. \quad (13)$$

Note that the prefactors in (12) ensure constant volume of the drop for all values of  $\epsilon_b, \epsilon_c$  in accordance with the experimental situation.

For an ellipsoid the magnetization in a homogeneous field is known to be homogeneous as well, hence the volume integral in (10) just gives rise to a factor  $V$ . Moreover the relation between the magnetization  $\mathbf{M}$ , the external field  $\mathbf{G}$  and the internal field  $\mathbf{H}$  in the ferrofluid is for our geometry given by [21]

$$G_x = H_x + 4\pi n_1 M_x, \quad G_y = H_y + 4\pi n_2 M_y, \quad (14)$$

where  $n_1$  and  $n_2$  denote the demagnetizing factors along the  $x$ - and  $y$ -axis, respectively, which are also known functions of  $\epsilon_b$  and  $\epsilon_c$  and can be expressed in terms of elliptic integrals [21].

Although the original problem is in this way substantially simplified, it is still impossible to derive a universally valid expression for the magnetic energy. To close the set of equations we need the magnetization law  $\mathbf{M} = \mathbf{M}(\mathbf{H}, \omega)$  describing the *dynamic response* of the ferrofluid in an external magnetic field. To obtain this law in full generality is a rather difficult task, both theoretically and experimentally. We will therefore use different approximations of increasing sophistication to determine the magnetic field energy. We start with the *linear response* assumption  $\mathbf{M} = \chi \mathbf{H}$  in the next subsection and proceed by including non-linear effects in Sect. 3.3.

For later convenience we introduce some auxiliary quantities originally due to Jeffrey [19], namely

$$n'_1 = -\frac{n_2 - n_3}{b^2 - c^2} \quad \text{and} \quad n''_1 = \frac{n_2 b^2 - n_3 c^2}{b^2 - c^2} \quad (15)$$

with analogous expressions for  $n'_2, n'_3, n''_2$  and  $n''_3$  following by cyclic permutations in 1, 2, 3 and  $a, b, c$ . Moreover we will use the demagnetizing factors  $\tilde{n}_1, \tilde{n}_2$  and  $\tilde{n}_3$  of the so-called *additional* ellipsoid defined by the semi-axes  $\tilde{a} = a, \tilde{b} = ac/b$  and  $\tilde{c} = c$ . Note that a prolate ellipsoid of revolution ( $a > b = c$ ) corresponds to an oblate additional ellipsoid of revolution ( $\tilde{a} = \tilde{b} > \tilde{c}$ ), and vice versa.

### 3.2. Linear Magnetization Law

For a sufficiently small external magnetic field the response of the ferrofluid will be linear. This implies that the magnetization shows the same harmonic time dependence as the external field, and the simple magnetization law

$$\mathbf{M} = \chi \mathbf{H} \quad (16)$$

with the complex susceptibility  $\chi = \chi_1 - i\chi_2$  is applicable.

Using (16), (14) and (11) we find for the magnetization

$$\mathbf{M} = G \Re \left\{ \chi \exp(i\omega t) \left( \frac{1}{1 + 4\pi\chi n_1}, \frac{-i}{1 + 4\pi\chi n_2}, 0 \right) \right\}. \quad (17)$$

The magnetic energy (10) can be further simplified according to

$$E_m(t) = -V \int_0^{\mathbf{G}(t)} d\mathbf{G}' \mathbf{M}(\mathbf{G}') = -\frac{V}{2} \mathbf{G} \cdot \mathbf{M}. \quad (18)$$

Substituting  $\mathbf{M} \rightarrow (\mathbf{M} + \mathbf{M}^*)/2$ , and  $\mathbf{G} \rightarrow (\mathbf{G} + \mathbf{G}^*)/2$ , this expression becomes the sum of four terms, two of which are constant in time and the remaining two oscillating with double frequency  $2\omega$ . After averaging  $E_m(t)$  over one period of the external field, the latter terms vanish and within the linear approximation we hence get for the average magnetic energy

$$\bar{E}_m = -\frac{VG^2}{4} \Re \{ L_1 + L_2 \} \quad (19)$$

with

$$L_i = \frac{\chi}{1 + 4\pi\chi n_i}, \quad i = 1, 2. \quad (20)$$

This result generalizes the one obtained previously for the case of negligible dispersion,  $\chi_2/\chi_1 \rightarrow 0$  [24].

Plugging (19) and (12) into (9) we obtain the total energy of the drop within the approximation of a linear magnetization law. The equilibrium shape is given by the minimum of this function with respect to the geometry parameters  $\epsilon_b$  and  $\epsilon_c$ . Putting the respective derivatives equal to zero we obtain two equations determining  $\epsilon_b$  and  $\epsilon_c$  for a given value of the magnetic field. Using the auxiliary quantities introduced in Subsect. 3.1, these equations can be written in the compact

form

$$\begin{aligned} \tilde{n}_1(a^2 - b^2) + c^2(\tilde{n}_3 - \tilde{n}_2) & \quad (21) \\ &= \frac{2\pi}{3}B [\Re\{L_1^2\}(n_2'' + 2n_3'') - \Re\{L_2^2\}(n_1'' + 2n_3'')] \end{aligned}$$

and

$$\begin{aligned} -\tilde{n}_1(a^2 + b^2) + \tilde{n}_2(2a^2 - c^2) + \tilde{n}_3(2b^2 - c^2) & \quad (22) \\ &= 2\pi B [\Re\{L_1^2\}n_2'' + \Re\{L_2^2\}n_1''], \end{aligned}$$

where the magnetic bond number  $B$  was defined in (8).

Before discussing the solution of these equations it is worthwhile to study the dependence on the material parameters  $\chi_1$  and  $\chi_2$ . These enter the expressions only via the quantities  $L_i$  and since

$$\Re\{L_i\} = \frac{\chi_1 + 4\pi n_i \chi_1^2 (1 + (\chi_2/\chi_1)^2)}{1 + 8\pi n_i \chi_1 + 16\pi^2 n_i^2 \chi_1^2 (1 + (\chi_2/\chi_1)^2)}, \quad (23)$$

the dependence on  $\chi_2$  is solely through the combination  $(\chi_2/\chi_1)^2$ . The ratio  $\chi_2/\chi_1$  becomes of order 1 only at rather high frequencies of about 10 kHz, where  $2\pi/\omega$  gets comparable to the Brownian relaxation time  $\tau_B$ . In our experiments the frequency of the magnetic field is much lower and  $\chi_2/\chi_1 \lesssim 0.1$ . Consequently we will neglect the influence of  $\chi_2$  on the *shape* of the drop and use from now on

$$L_i = \frac{\chi_1}{1 + 4\pi\chi_1 n_i}. \quad (24)$$

As we will see below, despite its smallness,  $\chi_2$  is crucial in the determination of the *rotation* of the drop. It is in order also to emphasize at this point that neglecting  $\chi_2$  does not imply to neglect the *dispersion* of the susceptibility all together. In fact the frequency dependence of the *real* part of the susceptibility,  $\chi_1 = \chi_1(\omega)$ , is quite substantial and has to be taken into account.

One solution of the system (21), (22) can be obtained analytically. It corresponds to an *oblate spheroid* characterized by  $a = b > c$ . In this case  $n_1 = n_2 = n$  and (21) becomes an identity, whereas (22) can be transformed into

$$B = 4\pi \left( \frac{1}{4\pi\chi_1} + n \right)^2 \frac{\epsilon_c^2 - 1}{\epsilon_c^{4/3}} \frac{2\epsilon_c^2 - 1 - \tilde{n}(4\epsilon_c^2 - 1)}{n(\epsilon_c^2 + 2) - 1}, \quad (25)$$

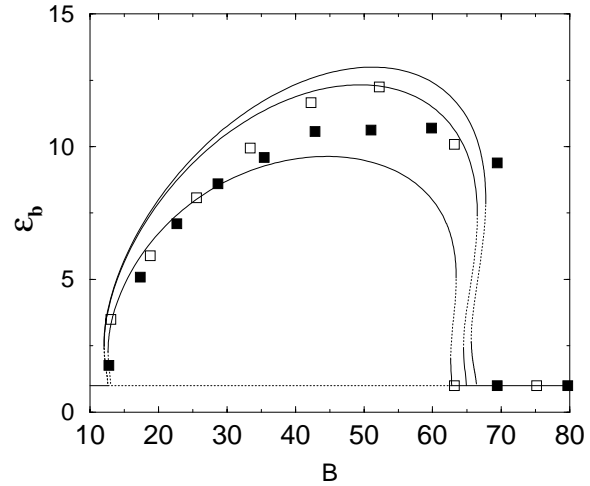


Fig. 2. Ratio  $\epsilon_b = a/b$  between the two largest semi-axes of a rotating ferrofluid drop as a function of the magnetic bond number  $B$  for the parameters specified in Table 1. The curves show from top to bottom the results for a linear magnetization law,  $\mathbf{M} = \chi\mathbf{H}$ , for the Langevin  $M(H)$  and for the dynamic curve  $M(H)$  as determined from an independent experiment. Full lines correspond to stable configurations, dotted lines to unstable ones. Symbols are experimental results with filled symbols corresponding to increasing, and empty symbols to decreasing field strength.

where  $\tilde{n}$  denotes the demagnetizing factor of the additional ellipsoid along its longest axis  $\tilde{a} > \tilde{b} = \tilde{c}$ . Equation (25) gives an explicit relation between the magnetic bond number  $B$  and the semi-axes ratio  $\epsilon_c$ . Starting with the spherical shape in zero field, this axis-symmetric solution describes the continuous flattening of the drop with increasing field.

For a given value of  $\omega$  this solution exists for all values of  $\chi_1$  and  $B$ . However, it is *stable* for all  $B$  only for sufficiently small values of  $\chi_1$ . In fact for  $\chi_1 > \chi_1^* = 0.325$  it loses its stability within a *bounded window* of intermediate values of  $B$  where a *non axis-symmetric* solution with  $a \neq b$  appears, see Figs. 2 and 3. Increasing the magnetic field strength the drop hence transforms from a spheroid at low values of  $B$  to a *three-axes ellipsoid* and back to a disc-like spheroid at high values of  $B$ . The first bifurcation is *supercritical* for  $\chi_1^* < \chi_1 < \chi_1^A = 0.843$ , the second one in the interval  $\chi_1^* < \chi_1 < \chi_1^B = 1.02$ . For larger values of  $\chi_1$  these bifurcations become *subcritical* and the transitions are accompanied by hysteresis. The situation is summarized by the stability dia-

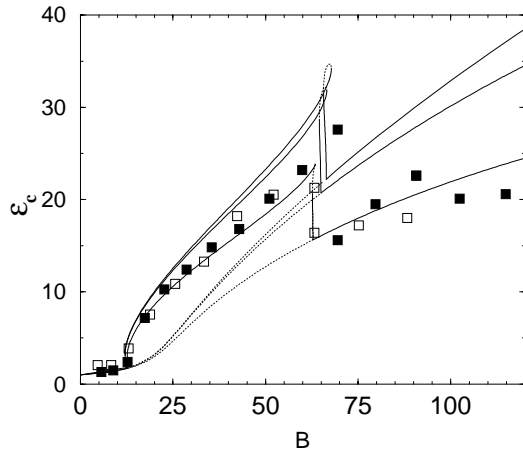


Fig. 3. Same as Fig. 2 for the ratio  $\epsilon_c = a/c$  between the largest and the smallest semi-axes of the rotating drop.

gram shown in Fig. 4. Also shown as dashed line is the theoretical result for the transition line in the strongly magneto-dissipative case  $\chi_2 = \chi_1$ , which describes the case of high frequency,  $\omega\tau_B \sim 1$ . As can be seen from Fig. 4 the region of non axis-symmetric shapes is much smaller in this case.

From Figs. 2, 3, and 4 it is apparent that the critical values of the magnetic bond number  $B$  at which the various shape bifurcations occur are qualitatively and also quantitatively well described by the above sketched theory assuming a linear magnetization law. The values of the eccentricities, however, are systematically overestimated, in particular for large values of  $B$ . The reason is rather simple. In our experimental setup a magnetic bond number of 50 corresponds to an external magnetic field of the order of the saturation magnetization  $M_\infty$  of the ferrofluid. Correspondingly saturation effects come into play and there are noticeable deviations from the linear magnetization law giving rise to smaller values of the magnetic energy. This in turn implies a reduction of the induced eccentricities of the drop.

### 3.3. Non-linear Magnetization Law

We now investigate the corrections to the results obtained above when considering more realistic magnetization laws including saturation effects. We will continue to assume that  $\mathbf{M}$  and  $\mathbf{H}$  are parallel. This neglects magneto-dissipative effects and is equivalent to the assumption  $(\chi_2/\chi_1)^2 \ll 1$  used in the linear case.

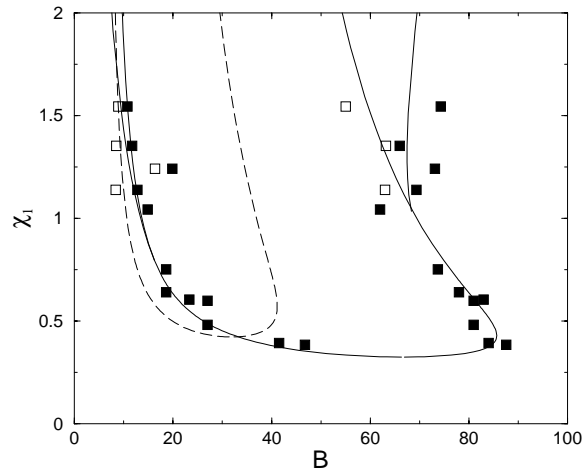


Fig. 4. Stability diagram of drop shapes in the  $B - \chi_1$ -plane assuming a linear magnetization law  $M = \chi H$ . Full lines are theoretical results for the transitions between the different shapes assuming  $\chi_2 = 0$ . Experimental results are shown as symbols with full (empty) symbols representing transitions in an increasing (decreasing) field. For small susceptibilities,  $\chi_1 < 0.325$ , there is a continuous transition from the initially spherical shape at zero field to a strongly flattened disk-like spheroid at large field. For intermediate values of  $\chi_1$ ,  $0.325 < \chi_1 < 0.843$ , a soft transition to a three-axis ellipsoid and back takes place. For large values of  $\chi_1$  these shape transformations occur via subcritical bifurcations with the corresponding opening of a hysteretic window at the transition lines. The dashed line is the transition line for the strongly magneto-dissipative case  $\chi_2 = \chi_1$ .

As a simple example of a non-linear magnetization law we first consider the standard Langevin law

$$M(H) = M_\infty L\left(\frac{3\chi_1}{M_\infty} H\right), \quad (26)$$

where  $L(\xi) = \coth(\xi) - 1/\xi$  denotes the Langevin function, and the initial susceptibility is set equal to its *experimental* value  $\chi_1$ , i. e. the value used already in the linear case. Afterwards we will employ a complete function  $M = M(H)$  derived from data obtained in an independent experiment.

The surface energy of the drop is, of course, the same as before. The determination of the magnetic energy is, however, more involved. Of central importance is again (14) which is valid also for non-linear magnetization laws.

For simplicity we start with the case of a spheroid,  $a = b > c$ . The surface area simplifies to

$$S = 2\pi R^2 \epsilon_c^{-4/3} \left[ \epsilon_c^2 + \frac{1}{2m} \ln \frac{1+m}{1-m} \right], \quad (27)$$

where  $m$  was defined in (13). Moreover  $n_1 = n_2 = n$ . To perform the integration over  $G$  in the calculation of the magnetic energy according to (10) it is convenient to use (14) in differential form to obtain

$$\begin{aligned} \frac{E_m}{V} &= - \int_0^{G(t)} d\mathbf{G}' \mathbf{M}(\mathbf{G}') \\ &= - \int_0^H d\mathbf{H}' \mathbf{M}(\mathbf{H}') - 4\pi n \int_0^M d\mathbf{M}' \mathbf{M}' \quad (28) \\ &= - \int_0^H dH' M(H') - 2\pi n M^2, \end{aligned}$$

which is *independent* of time. In the last step we used the assumption that  $\mathbf{M}$  and  $\mathbf{H}$  are parallel. For the Langevin law (26) the remaining integral can be calculated analytically:

$$\int_0^H dH' M(H') = \frac{M_\infty^2}{3\chi_1} \ln \frac{\sinh(3\chi_1 H/M_\infty)}{3\chi_1 H/M_\infty}. \quad (29)$$

From the variation of both (27) and (28) with respect to  $\epsilon_c$  we find the generalization of (25) in the form

$$\frac{4\pi M^2 R}{\alpha} = \frac{\epsilon_c^2 - 1}{\epsilon_c^{4/3}} \frac{2\epsilon_c^2 - 1 - \tilde{n}(4\epsilon_c^2 - 1)}{n(\epsilon_c^2 + 2) - 1}. \quad (30)$$

To transform this equation into a relation between the geometry factor  $\epsilon_c$  and the magnetic bond number  $B$  analogous to (25) we need to insert the relation between the magnetization  $M$  and the external field strength  $G$ . Neglecting magneto-dissipation, the external field  $\mathbf{G}$  and the internal field  $\mathbf{H}$  are parallel and we hence find from (14)

$$H + 4\pi n M(H) = G. \quad (31)$$

We therefore first calculate  $M$  as a function of  $\epsilon_c$  from (30). Using the relevant magnetization law  $M(H)$ , the corresponding value of  $G$  (or  $B$ , respectively) is then determined numerically using (31). The results obtained in this way are included in Fig. 3.

For a three-axis ellipsoid the situation is somewhat more complicated since  $\mathbf{G}$  and  $\mathbf{H}$  are no longer parallel. Denoting the angle between  $\mathbf{H}$  and the  $x$ -axis by  $\gamma$ , (14) can be written as (cf. Fig. 5)

$$G \cos(\omega t) = (H + 4\pi n_1 M(H)) \cos \gamma, \quad (32)$$

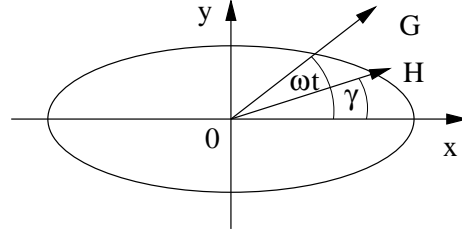


Fig. 5. Relative orientation of the external and internal magnetic field in the  $x$ - $y$ -plane for a non axis-symmetric drop.

$$G \sin(\omega t) = (H + 4\pi n_2 M(H)) \sin \gamma. \quad (33)$$

Eliminating the angle  $\gamma$  between these equations we obtain

$$\frac{1}{G^2} = \frac{\cos^2(\omega t)}{(H + 4\pi n_1 M(H))^2} + \frac{\sin^2(\omega t)}{(H + 4\pi n_2 M(H))^2}. \quad (34)$$

For a given magnetization law  $M(H)$ , this equation determines the internal field strength  $H$  and, using again  $M(H)$ , also the modulus of the magnetization as function of time. For non-trivial  $M(H)$  it has to be solved numerically *for every time moment*. The magnetic energy assumes the form

$$\begin{aligned} \frac{E_m(t)}{V} &= - \int_0^G (dG'_x M_x + dG'_y M_y) \\ &= - \int_0^H (dH'_x M_x + dH'_y M_y) \\ &\quad - 4\pi \int_0^M (dM'_x n_1 M'_x + dM'_y n_2 M'_y) \quad (35) \\ &= - \int_0^H dH' M(H') - 2\pi (n_1 M_x^2 + n_2 M_y^2). \end{aligned}$$

Using (32) and (33) to express  $M_x$  and  $M_y$  in terms of  $G$  and  $H$  we finally get

$$\begin{aligned} \frac{E_m(t)}{V} &= \\ &- \left[ \frac{G^2 M(H)}{2} \left( \frac{\cos^2(\omega t)}{H + 4\pi n_1 M(H)} + \frac{\sin^2(\omega t)}{H + 4\pi n_2 M(H)} \right) \right. \\ &\quad \left. - \frac{HM(H)}{2} + \int_0^H dH' M(H') \right]. \quad (36) \end{aligned}$$

This expression gives the time dependent magnetic energy for a general magnetization law  $M(H)$  neglecting

magneto-dissipation. For the linear case  $M = \chi_1 H$  the last two terms cancel and we recover (19) and (24).

The complete procedure to determine the shape for a non-linear magnetization law is hence as follows. For given geometry parameters  $\epsilon_b, \epsilon_c$  we calculate the surface energy and the demagnetizing factors  $n_1$  and  $n_2$ . We then solve (34) numerically to get  $H(t)$  as function of time for one period of the external field. Next we determine  $E_m(t)$  according to (36) and perform the time average numerically. The result is added to the surface energy and the total energy is minimized in  $\epsilon_b$  and  $\epsilon_c$ .

The results for the Langevin magnetization law are included in Figs. 2, 3. Although both  $\epsilon_b$  and  $\epsilon_c$  are reduced in comparison with the linear case, in particular  $\epsilon_c$  remains well above the experimental results.

We therefore conclude that the real magnetization law of the ferrofluid will deviate from the simple Langevin form. A useful starting point to determine a more realistic  $M(H)$  is given by the rather general relaxation equation for the magnetization [25–27]

$$\begin{aligned} \partial_t \mathbf{M} = & -\frac{1}{\tau_{\parallel} H^2} [\mathbf{H} \cdot (\mathbf{M} - \mathbf{M}_s(\mathbf{H}))] \mathbf{H} \\ & - \frac{1}{\tau_{\perp} H^2} \mathbf{H} \times (\mathbf{M} \times \mathbf{H}). \end{aligned} \quad (37)$$

Here  $\mathbf{M}_s(\mathbf{H})$  denotes the equilibrium magnetization corresponding to the magnetic field  $\mathbf{H}$ , and  $\tau_{\parallel}$  and  $\tau_{\perp}$  are the relaxation times of the magnetization parallel and perpendicular to the field  $\mathbf{H}$ , respectively. Equation (37) can be derived from an approximate solution of the Fokker-Planck equation describing the orientational Brownian motion of the ferromagnetic particles [25, 26] and therefore includes both relaxation and saturation.

For the present problem we are interested in the solution for the magnetization component parallel to the internal field  $\mathbf{H}$  in a rotating external field  $\mathbf{G}$ . It is given by

$$M = \frac{M_s}{1 + \omega^2 \tau_{\parallel} \tau_{\perp}}, \quad (38)$$

where the relaxation times of the magnetization component parallel and perpendicular to the magnetic field are of the form [25, 26]

$$\tau_{\parallel} = \frac{H}{M_s} \frac{dM_s}{dH} \tau_B \quad (39)$$

and

$$\tau_{\perp} = \frac{2M_s}{3\chi_s H - M_s} \tau_B, \quad (40)$$

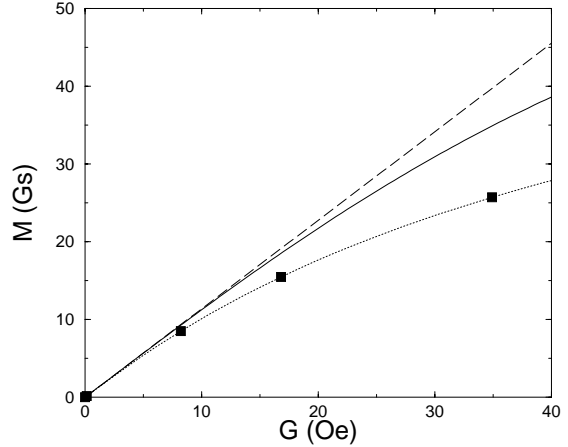


Fig. 6. Comparison of the three magnetization laws considered in the experimentally relevant interval of external field values. The dashed line is the linear law, the full line the Langevin law, and the dotted line the spline interpolation of the experimental values shown as squares. An external field of 39 Oe corresponds to a magnetic bond number  $B \simeq 150$ .

respectively. Here  $\chi_s = dM_s/dH|_{H=0}$  is the *static* susceptibility. In the limit  $H \rightarrow 0$  we find from these equations

$$(\omega \tau_B)^2 = \frac{\chi_s}{\chi_1} - 1, \quad (41)$$

which can be used to eliminate  $\tau_B$  in (39) and (40) to find

$$M = \frac{M_s}{1 + 2 \frac{(\chi_s/\chi_1 - 1) dM_s/dH}{3\chi_s - M_s/H}}. \quad (42)$$

This equation opens the interesting possibility to determine the *dynamic* magnetization curve  $M(H)$  relevant for the experiment from the *static* magnetization law  $M_s(H)$  and the real part of the susceptibility  $\chi_1(\omega)$  at the frequency  $\omega$  of the rotating magnetic field. Both  $M_s(H)$  and  $\chi_1(\omega)$  are easily accessible experimentally.

We have therefore determined the static magnetization curve  $M_s(H)$  of our ferrofluid in an independent experiment and have renormalized the data according to (42). In Fig. 6 a spline interpolation of the resulting  $M(H)$  is included. The deviations from the Langevin law are apparent.

Using the same spline interpolation in the numerical code to determine the shape of the drop, the results

represented by the lower curves in Figs. 2, 3 where obtained. As expected, the results for  $\epsilon_b$  and  $\epsilon_c$  are again reduced. For  $\epsilon_b$  this reduction is too large such that the experimental results are now underestimated. For  $\epsilon_c$  the agreement with the experiment is rather good, in particular for large values of the magnetic bond number. Note that in both figures there are no fit parameters.

#### 4. The Rotational Motion of the Drop

##### 4.1. General Remarks

We now turn to the second part of the problem. For given shape of the drop we aim at determining the angular velocity  $\Omega$  describing the rotation of the drop relative to the laboratory frame. The general strategy was outlined in Section 2. In the co-moving coordinate system we have to describe a liquid drop of *stationary shape* in an external flow field  $\mathbf{v}^{(e)}$  with the asymptotic behaviour

$$\mathbf{v}^{(e)} \rightarrow -\Omega \times \mathbf{r} = (y\Omega, -x\Omega, 0) \quad \text{for } r \rightarrow \infty. \quad (43)$$

In accordance with the assumed ellipsoidal shape of the drop we assume for the internal flow field (in the co-moving coordinate system) the simple form

$$\mathbf{v}^{(i)} = \left( -\zeta y \frac{a}{b}, \zeta x \frac{b}{a}, 0 \right) \quad (44)$$

with uniform vorticity

$$\frac{1}{2}(\nabla \times \mathbf{v}^{(i)}) = \frac{\zeta}{2} \left( 0, 0, \frac{a}{b} + \frac{b}{a} \right). \quad (45)$$

The stationary flow fields  $\mathbf{v}^{(i)}$  and  $\mathbf{v}^{(e)}$  inside and outside the drop, respectively, have to obey the equations (3). From (44) it follows that

$$p^{(i)} = \text{const.} \quad (46)$$

Denoting by  $\boldsymbol{\nu}$  the normal vector on the drop surface pointing outwards, the boundary conditions for the velocity fields at the surface of the drop are

$$\mathbf{v}^{(i)} \cdot \boldsymbol{\nu} = \mathbf{v}^{(e)} \cdot \boldsymbol{\nu} = 0 \quad \text{and} \quad \mathbf{v}^{(i)} \times \boldsymbol{\nu} = \mathbf{v}^{(e)} \times \boldsymbol{\nu}. \quad (47)$$

Writing the external flow field in the form

$$\mathbf{v}^{(e)} = \mathbf{v}^{(i)} + \mathbf{v}^{(J)} \quad (48)$$

and taking into account the boundary conditions (47) we infer that  $\mathbf{v}^{(J)} = (u^{(J)}, v^{(J)}, w^{(J)})$  describes the

Stokes approximation of a viscous flow field around a stationary, *rigid* ellipsoid with asymptotics

$$\mathbf{v}^{(J)} \rightarrow \left( y \left( \Omega + \zeta \frac{a}{b} \right), -x \left( \Omega + \zeta \frac{b}{a} \right), 0 \right) \quad (49)$$

for  $r \rightarrow \infty$ .

This is a classical problem in hydrodynamics which was solved by Jeffrey a long time ago [19]. The solution is parameterized in terms of the asymptotic velocity-gradient tensor

$$\lim_{r \rightarrow \infty} \frac{\partial v_i^{(J)}}{\partial x_k} = \gamma_{ik} + \omega_{ik} \quad (50)$$

decomposed into its symmetric and antisymmetric part  $\gamma_{ik}$  and  $\omega_{ik}$ , respectively. In our case we find from (49) for the relevant components of this tensor

$$\gamma_{12} = \gamma_{21} = \frac{\zeta}{2} \left( \frac{a}{b} - \frac{b}{a} \right) \quad (51)$$

$$\omega_{12} = -\omega_{21} = \Omega + \frac{\zeta}{2} \left( \frac{a}{b} + \frac{b}{a} \right). \quad (52)$$

In the way outlined above the problem of the hydrodynamic flow associated with the drop rotation is hence reduced to the determination of the so far unspecified parameters  $\Omega$  and  $\zeta$ . As explained in Sect. 2, the necessary two equations result from the balance of viscous and magnetic torques on the drop and from the integrated balance of tangential stresses at the surface of the drop. In the present subsection we determine the viscous contributions to these equations. The terms arising from the magnetic field are discussed in the subsequent subsections.

For symmetry reasons only the  $z$ -component of the viscous torque on the drop is different from zero. It is given by

$$L_z^v = \int_{\partial V} dS (xF_y - yF_x), \quad (53)$$

where  $\mathbf{F}$  denotes the force on an element  $dS$  of the drop surface, and the integral is over the complete surface of the drop. This force can be expressed in terms of the viscous stress tensor of the external flow as

$$F_i = \sigma_{ik}^{(e)} \nu_k. \quad (54)$$

From Jeffrey's solution we find for the contribution of  $\mathbf{v}^{(J)}$  to the force [19] (see also [28]),

$$F_i^{(J)} = -p\nu_i + \eta^{(e)} A_{ik} \nu_k. \quad (55)$$

Here  $p$  is a constant which will not contribute to the final result, and the  $A_{ik}$  are linear functions of the velocity-gradient tensor of the external flow. The elements relevant for our geometry are

$$A_{12} = 2 \frac{n_1 \gamma_{12} + b^2 n_3' \omega_{12}}{(a^2 n_1 + b^2 n_2) n_3'}, \quad (56)$$

where  $n_3'$  is defined by (15). The value of  $A_{21}$  is obtained from  $A_{12}$  by the replacements  $1 \leftrightarrow 2$  and  $a \leftrightarrow b$ .

Inserting (54),(55),(48) and (44) into (53) and using

$$\int_{\partial V} dS r_i \nu_k = V \delta_{ik} \quad (57)$$

as valid for integrals over the surface of an ellipsoid, we find

$$L_z^v = V \eta^{(e)} (A_{21} - A_{12}). \quad (58)$$

Note that the  $A_{ik}$  depend on  $\Omega$  and  $\zeta$  via (56) and (51), (52).

For the viscous contribution to the integrated balance of tangential stresses (7) we have to calculate

$$\mathbf{\Pi}^{(v)} = \int_{\partial V} dS (v_i^{(i)} \sigma_{ik}^{(i)} - v_i^{(e)} \sigma_{ik}^{(e)}) \nu_k. \quad (59)$$

From (44) and (48) we find for the relevant components of the viscous stress tensors of the internal and external flow *at the surface of the drop*

$$\begin{aligned} \sigma_{12}^{(i)} &= \eta^{(i)} \left( \frac{\partial v_1^{(i)}}{\partial x_2} + \frac{\partial v_2^{(i)}}{\partial x_1} \right) \\ &= \eta^{(i)} \zeta \left( \frac{b}{a} - \frac{a}{b} \right), \end{aligned} \quad (60)$$

$$\begin{aligned} \sigma_{12}^{(e)} &= \eta^{(e)} \left( \frac{\partial v_1^{(e)}}{\partial x_2} + \frac{\partial v_2^{(e)}}{\partial x_1} \right) \\ &= \eta^{(e)} \left( \zeta \left( \frac{b}{a} - \frac{a}{b} \right) + A_{12} \right). \end{aligned} \quad (61)$$

Using the continuity of the flow at the drop surface we finally get with the help of (57)

$$\begin{aligned} \mathbf{\Pi}^{(v)} &= (\eta^{(i)} - \eta^{(e)}) \zeta^2 V \left( \frac{b}{a} - \frac{a}{b} \right)^2 \\ &\quad + \eta^{(e)} \zeta V \left( \frac{a}{b} A_{12} - \frac{b}{a} A_{21} \right). \end{aligned} \quad (62)$$

#### 4.2. Linear Magnetization Law

To complete the analysis of the drop rotation we have to calculate the  $z$ -component of the magnetic torque on the drop and the magnetic contributions to the tangential stresses at the drop surface. As in the case of the shape problem we start with the case of a linear magnetization law (16).

The magnetic torque is given by [21]

$$\mathbf{L}^m = \int_V d^3r \mathbf{M} \times \mathbf{G}, \quad (63)$$

and for a homogeneously magnetized drop we find for the  $z$ -component

$$L_z^m = V (M_x G_y - M_y G_x). \quad (64)$$

As discussed in Sect. 2, our experimental setup is characterized by  $\Omega \ll \omega$ , and we may hence use (11) as time dependence of the external field also in the coordinate system rotating with angular velocity  $\Omega$ . Using (17) and performing similar manipulations as following (18) we find for the average of (64) over one period of the external field

$$\bar{L}_z^m = \frac{VG^2}{2} \chi_2 \left( \frac{1}{|1 + 4\pi\chi n_1|^2} + \frac{1}{|1 + 4\pi\chi n_2|^2} \right). \quad (65)$$

The time averaged magnetic torque  $\bar{L}_z^m$  is directly proportional to the imaginary part  $\chi_2$  of the susceptibility. This is physically reasonable, since in the absence of magneto-dissipation no average torque arises. Nevertheless we may use in (65) the leading terms of the results for  $n_1$  and  $n_2$  as obtained from the analysis of the shape, i.e. those *neglecting*  $\chi_2$ . To the same accuracy we can make the replacement  $\chi \rightarrow \chi_1$  in the denominators in (65). This gives finally rise to

$$\bar{L}_z^m = \frac{VG^2}{2} \chi_2 \left( \frac{1}{(1 + 4\pi\chi_1 n_1)^2} + \frac{1}{(1 + 4\pi\chi_1 n_2)^2} \right). \quad (66)$$

The magnetic contributions to the tangential stresses

$$\mathbf{\Pi}^{(m)} = \int_{\partial V} dS (v_i^{(i)} \sigma_{ik}^{(m,i)} - v_i^{(e)} \sigma_{ik}^{(m,e)}) \nu_k \quad (67)$$

follow from the magnetic stress tensor (1). Due to the boundary conditions for the magnetic fields  $\mathbf{H}$  and  $\mathbf{B}$

the Maxwell term  $H_i B_k / (4\pi)$  is the same inside and outside the drop and therefore does not contribute. The only contribution stems from the Shliomis term describing the non-equilibrium character of the drop magnetization. Using that both  $\mathbf{M}$  and  $\mathbf{H}$  are homogeneous inside the drop and employing again (57) we therefore find

$$\begin{aligned} \mathbf{\Pi}^{(m)} &= \frac{1}{2} \int_{\partial V} dS v_i^{(i)} (M_i H_k - M_k H_i) \nu_k \\ &= \frac{1}{2} (M_i H_k - M_k H_i) \int_{\partial V} dS v_i^{(i)} \nu_k \quad (68) \\ &= \frac{V}{2} \zeta (M_2 H_1 - M_1 H_2) \left( \frac{a}{b} + \frac{b}{a} \right). \end{aligned}$$

Averaging this result over one period of the magnetic field and using again the approximation  $\chi \simeq \chi^* \simeq \chi_1$  we get

$$\begin{aligned} \bar{\mathbf{\Pi}}^{(m)} &= \frac{VG^2}{2} \zeta \chi_2 \left( \frac{a}{b} + \frac{b}{a} \right) \\ &\cdot \frac{1}{(1 + 4\pi\chi_1 n_1)(1 + 4\pi\chi_1 n_2)}. \quad (69) \end{aligned}$$

Putting the sum of (58) and (66) as well as the sum of (62) and (69) equal to zero, we finally obtain the two required equations between  $\zeta$  and  $\Omega$ :

$$A_{12} - A_{21} = \frac{\chi_2 G^2}{2\eta^{(e)}} \left[ \frac{1}{(1 + 4\pi\chi_1 n_1)^2} + \frac{1}{(1 + 4\pi\chi_1 n_2)^2} \right], \quad (70)$$

$$\begin{aligned} \frac{a}{b} A_{12} - \frac{b}{a} A_{21} - \zeta \left( 1 - \frac{\eta^{(i)}}{\eta^{(e)}} \right) \left( \frac{b}{a} - \frac{a}{b} \right)^2 &= \\ \frac{\chi_2 G^2}{2\eta^{(e)}} \left( \frac{a}{b} + \frac{b}{a} \right) \frac{1}{(1 + 4\pi\chi_1 n_1)(1 + 4\pi\chi_1 n_2)}. \quad (71) \end{aligned}$$

Given the geometry and the material parameters, this is a system of two linear equations for  $\zeta$  and  $\Omega$  which determine their dependence on the magnetic bond number  $B$ . The results for  $\Omega$  for the parameters given in Table 1 are shown in Fig. 7 together with experimental results. Similar to the shape problem we find that the magnetic torque is overestimated by assuming a linear magnetization law resulting in a too high rotation frequency. It is therefore tempting to again investigate the influence of saturation effects, which is done in the next subsection.

### 4.3. Non-linear Magnetization Law

In the last section we found that for a linear magnetization law both the magnetic torque (66) and the magnetic contribution to the tangential stress (69) are proportional to  $\chi_2$ , i.e. for both quantities magneto-dissipative effects are important. The generalization of the simple law  $\mathbf{M} = \chi\mathbf{H}$  with complex susceptibility  $\chi$  to a non-linear dependence  $\mathbf{M}(\mathbf{H})$  including magneto-dissipative effects is much more complicated than for the situation neglecting magneto-dissipation discussed in Section 3.3.

A useful starting point is again the relaxation equation for the magnetization (37). For a given time dependence of the external field  $\mathbf{G}$  it can be combined with (14) to yield the following differential equations for the components of the internal magnetic field

$$\begin{aligned} \partial_t H_x &= - \left[ \frac{1}{\tau_\perp} + \left( \frac{1}{\tau_\perp} - \frac{1}{\tau_\parallel} \right) \frac{1}{H^2} \left( H_x G_x - H_x^2 \right. \right. \\ &\quad \left. \left. + \frac{n_1}{n_2} (H_y G_y - H_y^2) \right) + \frac{4\pi n_1 M_s(H)}{\tau_\parallel H} \right] H_x \\ &\quad - G \sin(\omega t) + \frac{G}{\tau_\perp} \cos(\omega t), \quad (72) \end{aligned}$$

$$\begin{aligned} \partial_t H_y &= - \left[ \frac{1}{\tau_\perp} + \left( \frac{1}{\tau_\perp} - \frac{1}{\tau_\parallel} \right) \frac{1}{H^2} \left( H_y G_y - H_y^2 \right. \right. \\ &\quad \left. \left. + \frac{n_2}{n_1} (H_x G_x - H_x^2) \right) + \frac{4\pi n_2 M_s(H)}{\tau_\parallel H} \right] H_y \\ &\quad + G \cos(\omega t) + \frac{G}{\tau_\perp} \sin(\omega t). \quad (73) \end{aligned}$$

For a given static magnetization law  $M_s(H)$  these equations can be solved numerically. Starting with a sensible initial condition, the stationary regime is reached after a few periods of the external field. From the results for  $H_x(t)$  and  $H_y(t)$  the time dependence of  $M_x$  and  $M_y$  can be obtained using once more (14). Plugging the results into (64) and (68) and performing the remaining time average numerically we find again two linear equations for  $\Omega$  and  $\zeta$ . The results for  $\Omega(B)$  obtained in this way for the magnetization curve as determined in an independent experiment are included in Figure 7.

From the figure it is seen that the rotation frequency is slightly reduced in comparison with the results for a linear magnetization law. This is in accordance with

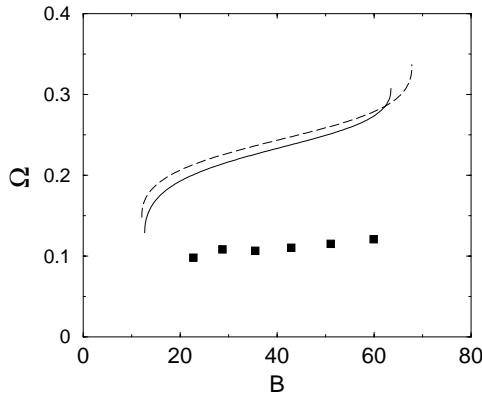


Fig. 7. Rotation frequency of the drop in  $s^{-1}$  as function of the magnetic bond number. Squares are experimental values, lines are theoretical results using a linear magnetization law (dashed) and the magnetization curve  $M(H)$  as determined in an independent experiment (full), respectively.

intuition since due to the saturation of the magnetization the magnetic torque is reduced and correspondingly the rotation is slowed down. However, the reduction of  $\Omega$  is much smaller than might have been expected when simply estimating the change in the magnetic torque. The reason is that also the eccentricities of the drop become smaller (cf. Figs. 2 and 3) inducing a reduction of the viscous torque as well. As a combined outcome of a smaller magnetic and a smaller viscous torque the rotation frequency remains nearly unchanged.

In conclusion we found that also the rotation frequency calculated from a non-linear magnetization law strongly overestimates the experimental results for  $\Omega$ . We therefore expect that other effects than the saturation of the magnetization are more efficient in slowing down the rotation of the drop. Possible candidates are the multi-dispersedness of the ferrofluid reducing the magnetic torque and deviations from the elliptic shape increasing the viscous one. Let us also stress again that in Fig. 7 no fit parameters were used and that a rather good agreement between theory and experiment could be obtained by fitting, e.g., the Brownian relaxation time  $\tau_B$  of the ferrofluid.

#### 4.4. Rotating Spheroid in High Field

It is quite interesting to consider the rotation of the oblate spheroid that develops for large values of the external field strength. In this case we have  $a = b$  and

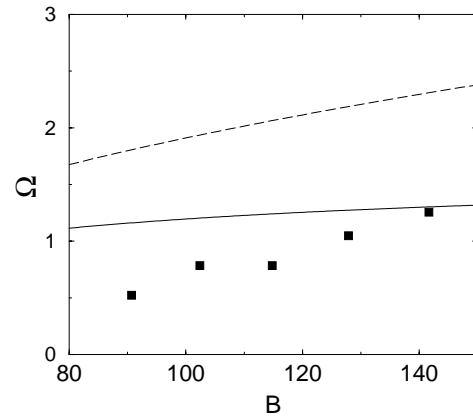


Fig. 8. Rotation frequency in  $s^{-1}$  of a disk-like drop as function of the magnetic bond number. Squares are experimental values, lines are theoretical results using a linear magnetization law (dashed) and the magnetization curve  $M(H)$  as determined in an independent experiment (full), respectively.

consequently  $n_1 = n_2 =: n$ . The two equations for  $\zeta$  and  $\Omega$  resulting from the balance of torques and the integrated balance of tangential stresses at the surface of the drop *coincide* and give rise to *one* equation for the sum  $\Omega + \zeta$  only. This is easily verified for the case of a linear magnetization law where both (70) and (71) reduce to

$$\Omega + \zeta = \frac{\chi_2 G^2}{2\eta^{(e)}} \frac{n}{(1 + 4\pi\chi_1 n)^2}. \quad (74)$$

For a spheroid it is hence impossible to determine  $\Omega$  and  $\zeta$  independently and only the sum  $\Omega + \zeta$  has a definite meaning. This is in accordance with the fact that  $\Omega$  was introduced as the rotation frequency of the *shape* of the drop which is not unambiguously defined for a spheroid. Instead, the sum  $\Omega + \zeta$  describes the *rigid body* rotation of the drop in the laboratory frame.

On the experimental side it is rather difficult to reliably measure the rotation of the spheroid. This is the reason why we have no experimental results for the rotation frequency at small field values where the drop has still its spheroidal shape. However, as explained in Sect. 5 (see Fig. 1), the peaks at the periphery of the drop in *large* fields allow to determine the rotation frequency in this regime.

In Fig. 8 we give a comparison of theoretical and experimental results for the rotation of a disk-like drop at high field values. The reduction due to the saturation effects is now more pronounced. For smaller values of  $B$  there are few and large peaks at the pe-

riphery of the drop, increasing the viscous torque significantly. Accordingly the rotation frequency remains well below the theoretical values. With increasing field strength, however, the peaks become more numerous and smaller (see Fig. 1), such that our theoretical model of a spheroid is again more realistic. In this regime the theoretical results for a non-linear magnetization law agree well with the experiment.

## 5. Experiments

In our experiments we have used a kerosene-based magnetic fluid with dispersed magnetite particles of about 10 nm diameter stabilized with oleic acid. The ferrofluid has a static magnetic susceptibility  $\chi_s \approx 1.91$  and a density  $\rho_m = 1.8 \text{ g/cm}^3$ . Diluting this original fluid with pure kerosene we prepared 12 samples of magnetic fluids with susceptibilities between 0.31 and 1.54. The corresponding densities varied between  $1.2 \text{ g/cm}^3$  and  $1.75 \text{ g/cm}^3$ .

As fluid surrounding the drops we chose 3-bromo-1,2-propanediol with a density  $\rho_p = 1.8 \text{ g/cm}^3$ . It can be diluted by pure water to reduce its density up to the value matching the density of the ferrofluid under consideration. The main advantage of 3-bromo-1,2-propanediol compared to other possible liquids is that its interface with the ferrofluid remains stable and of constant physical properties for several days.

The experiments start with the preparation of the appropriate density and density gradient of the external fluid. To this end 3-bromo-1,2-propanediol is filled into a glass container with the size  $5 \times 5 \times 6 \text{ cm}$ , and an appropriate amount of water is added to the top of the fluid. After 1-2 days a slight concentration gradient develops which is necessary to keep the ferrofluid drop near the center of the container. With a syringe a ferrofluid drop with a radius  $R$  between 0.2 and 0.5 cm is placed in the center of the container which, usually after a slight adaption of its height, remained stationary and spherical. Note that the concentration gradient in the surrounding liquid must be sufficiently small to leave the equilibrium shape of the drop spherical.

The container is placed between two perpendicular pairs of Helmholtz coils producing the external magnetic field  $\mathbf{G}$ . The pairs are operated with an alternating current of frequency  $f = 560 \text{ Hz}$  and a relative phase shift of  $\pi/2$  resulting in a rotating magnetic field with angular frequency  $\omega = 3520 \text{ s}^{-1}$ . The typical frequency of the drop rotation is  $\Omega/2\pi \sim 0.1 \text{ Hz}$ , and hence the condition  $\Omega \ll \omega$  is very well satisfied in

Table 1. Parameter values relevant for the experimental results reported in Figs. 2, 3, 7, and 8.

$R$ cm	$\chi_s$	$\chi_1$	$\chi_2$	$M_\infty$ (Gs)	$\eta^{(i)}$ (P)	$\eta^{(e)}$ (P)	$\alpha$ (dyn/cm)
0.275	1.35	1.14	0.17	80	0.19	0.58	2.8

the experiment. The magnetic field is uniform within a deviation of less than 1 % in an approximately cylindrical region of diameter 4 cm and height 8 cm, so the ferrofluid drop always experiences a spatial homogeneous field. The maximum field amplitude is about 50 Oe.

Before starting the main experiment the parameters of the system were determined by independent measurements. First the static magnetization curve  $M(H)$  was recorded, yielding the initial static susceptibility  $\chi_s$  and the saturation magnetization  $M_\infty$ . Second the *dynamic* susceptibilities  $\chi_1$  and  $\chi_2$  were determined for an alternating magnetic field with the experimentally relevant frequency  $f = 560 \text{ Hz}$ . In all cases  $\chi_2$  was by a factor 7 to 10 smaller than  $\chi_1$  such that the condition  $(\chi_2/\chi_1)^2 \ll 1$  holds. Third the dynamic viscosities  $\eta^{(i)}$  and  $\eta^{(e)}$  of the ferrofluid and the external fluid, respectively, were determined by standard rheological methods. Even for the highest viscosities measured, the fluids behaved as Newtonian liquids. The accuracy in the experimental determination or control of the magnetic field strength  $G$ , the susceptibilities  $\chi_s$ ,  $\chi_1$  and  $\chi_2$  and the static magnetization curve  $M_s(H)$  was better than 1%. The interface tension  $\alpha$  was determined by measuring the elongation of the drop in a *static* external field [12]. The typical values of  $\alpha$  obtained range from 2 to 5 dyn/cm. This is comparable to many common fluids and three orders of magnitude higher than the unusually small interface tension characteristic for the micro-drops used in the experiments reported in [7, 12, 17]. As usual it is quite hard to determine the interface tension reliably. The accuracy in our determination of  $\alpha$  was about 3–5% for the diluted samples ( $\chi \simeq 0.3$ ) and about 7–10% in the case of concentrated ferrofluids ( $\chi \simeq 1.8$ ). The parameter values for the main experiments discussed in the present paper are collected in Table 1. The uncertainty about the exact value of  $\alpha$  translates into an error for the magnetic bond number  $B$  of about 7% in Figs. 2, 3, 7, and 8.

After these preparatory investigations the behaviour of the drops in a rotating magnetic field of variable amplitude was investigated in the main experiment. Starting with a spherical shape at zero field we observed for all investigated susceptibilities an initial flattening of

the drop in the vertical direction, i.e. perpendicular to the field plane when the field amplitude increased. For the most diluted sample with  $\chi_1 \approx 0.31$  this flattening smoothly continued up to the highest investigated field amplitudes. All other drops in our experiments had susceptibilities  $\chi_1 > \chi_1^* \approx 0.325$  and showed a transition to a non axis-symmetric state resembling a three-axis ellipsoid for intermediate values of the magnetic field strength. If  $\chi_1 < 1.14$  the transitions occurred for increasing and decreasing field at the same values of the field amplitude. For still higher susceptibilities both transitions showed hysteresis. These results are shown by the symbols in Fig. 4 and agree well with the theoretical investigations described above.

We emphasize that for *fixed* field amplitude the corresponding shape of the drop remains *stationary*. This is in marked contrast to the experiments with microdrops reported in [7, 17] and allows for the first time a detailed comparison between theory and experiment for the non axis-symmetric state. For a setup with parameters as specified in Table 1 we recorded the semi-axes ratios  $\epsilon_b = a/b$  and  $\epsilon_c = a/c$  as functions of the magnetic bond number  $B$ . The results are displayed in Figs. 2 and 3. The hysteresis is clearly seen for the transition in high field,  $B \sim 65$ . Moreover the steep increase of  $\epsilon_b$  at the low field transition,  $B \sim 15$ , indicates a hard transition here as well. The ratio  $\epsilon_c$  between the largest and the smallest semi-axes describes the flattening of the drop perpendicular to the field plane, interrupted by the transition to the non axis-symmetric shape at intermediate values of the field amplitude. The error in the measurement of the semi-axes is below 1% as long as there are no peaks at the periphery. When peaks show up, the semi-axes were determined from an average over the the maxima and minima of these peaks. The experimental error for the resulting values of  $a$  and  $b$  may be estimated between 7–10% for the case of a few large peaks and 2–3% for drops with many small peaks.

For non axis-symmetric shapes the experimental determination of the slow rotation frequency  $\Omega$  of the drop shape is easy since the ratio  $a/b$  is in general rather large. The corresponding results are shown by the symbols in Figure 7. For the spheroidal shape in low field it is very hard to measure the rotation frequency reliably. On the other hand the disk-like drops at large fields develop peaks at the periphery due to the normal field instability [10] which renders the experimental determination of the rigid body rotation frequency of the drop again possible (cf. Fig. 1). The ex-

perimental results for the rotational motion obtained for sufficiently large field amplitudes are displayed in Figure 8. The experimental error for the values of  $\Omega$  was again less than 1%.

## 6. Conclusion

In the present paper we have theoretically and experimentally investigated the stationary shapes and the motion of rotating ferrofluid drops. The drops are immersed in a non-magnetic liquid of the same density and spun up by a rotating external magnetic field of high frequency. To make the problem theoretically tractable we have introduced several approximations which describe the experimental situation rather well. Most notably the drop shape was approximated as a three-axes ellipsoid and the hydrodynamics were described within the Stokes approximation.

The most striking effect concerning the shape of the drop is a transition from an oblate spheroid to a *non axis-symmetric* form and back when the magnetic field strength is increased. This scenario occurs only when the susceptibility of the ferrofluid is sufficiently large,  $\chi > \chi^* \approx 0.325$ . The shape transformations occur in a soft way via forward bifurcations for susceptibilities not too different from  $\chi^*$  and show a hysteretic behaviour corresponding to backward bifurcations for large susceptibilities. The complete phase diagram is in good agreement with our experimental results (Fig. 4). Our value of the critical susceptibility  $\chi^*$  is significantly smaller than the result  $\chi^* \approx 0.56$  given in [7].

Our experiments are characterized by parameters (cf. Table 1) which ensure that all occurring drop shapes are *stationary*. This enabled us to perform for the first time a detailed comparison between theory and experiment in the non axis-symmetric regime. As shown in Figs. 2 and 3, *quantitative* agreement between theory and experiment can be obtained if the non-linear character of the magnetization law of the ferrofluid is taken into account. All parameters of our experimental setup were determined in independent experiments, so that there are no fit parameters.

Whereas the rotational motion of the axis-symmetric drop is difficult to determine experimentally, the slow rotation of the elongated non axis-symmetric shape is easy to monitor. Our theoretical analysis uses the superposition principle following from the Stokes approximation and builds on Jeffrey's classical solution for the viscous flow around a

rigid ellipsoid. Theory and experiment agree qualitatively for the whole range of field values. Quantitative agreement was, however, only obtained for rather large field amplitudes, where the rotation of the then again spheroidal drop can be observed due to Rosensweig peaks at the drop periphery.

To summarize, we have shown that ferrofluid drops are a convenient tool to study the equilibrium shapes of rotating bodies, both experimentally and theoretically. Choosing suitable parameter combinations, various transitions between stationary shapes of different symmetry as well as different rotation regimes of the drop can be observed and analyzed.

### Appendix A

In this appendix we prove the equivalence of the energy dissipation balance in the system and the integrated balance of tangential stresses (7). We denote by  $W_1$  and  $W_2$  the dissipation rate per unit time due to the viscous flows inside and outside the drop respectively, by  $W_m$  the rate of magneto-dissipation due to the periodic re-magnetizations of the ferrofluid, and by  $W_G$  the power input from the external magnetic field. All quantities are defined in the *laboratory* coordinate system  $\Sigma$ , and it is understood that they are averaged over one period of the external field. In the stationary state we must clearly have

$$W_G = W_1 + W_2 + W_m. \quad (\text{A1})$$

For the power input from the external field per volume we know [21]

$$\frac{W_G}{V} = -\overline{\mathbf{M} \frac{d\mathbf{G}}{dt}}, \quad (\text{A2})$$

and using (14) this can be written as

$$\frac{W_G}{V} = -\overline{\mathbf{M} \frac{d\mathbf{H}}{dt}} - 4\pi \overline{M_i \frac{d(n_{ik} M_k)}{dt}}, \quad (\text{A3})$$

where the time dependence of the demagnetizing tensor  $n_{ik}$  in the laboratory frame has to be taken into account.

We will analyze the two terms on the rhs of (A3) separately. To this end we discuss the first one in the coordinate system  $\Sigma'$  rotating relative to the laboratory frame with the angular velocity  $\boldsymbol{\Omega}'$  equal to the fluid vorticity inside the drop. Using (45) for the vorticity in the system rotating with angular velocity  $\boldsymbol{\Omega}$  relative to

the laboratory frame, we get

$$\boldsymbol{\Omega}' = \left( 0, 0, \Omega + \frac{\zeta}{2} \left( \frac{a}{b} + \frac{b}{a} \right) \right). \quad (\text{A4})$$

From the standard transformation of the time derivative of a vector quantity  $\mathbf{A}$  from  $\Sigma$  to  $\Sigma'$  given by

$$\frac{d\mathbf{A}}{dt} = \frac{d'\mathbf{A}}{dt} + \boldsymbol{\Omega}' \times \mathbf{A} \quad (\text{A5})$$

we find

$$-\overline{\mathbf{M} \frac{d\mathbf{H}}{dt}} = -\overline{\mathbf{M} \frac{d'\mathbf{H}}{dt}} + \boldsymbol{\Omega}' \cdot \overline{(\mathbf{M} \times \mathbf{H})}. \quad (\text{A6})$$

Since there is no macroscopic vorticity of the ferrofluid in  $\Sigma'$ , the first term on the rhs of this equation is to be identified with the dissipation rate  $W_m/V$  due to the relaxation of the magnetization.

Using (A4) we therefore find for the first term on the rhs of (A3)

$$-\overline{\mathbf{M} \frac{d\mathbf{H}}{dt}} = \frac{W_m}{V} + \left[ \Omega + \frac{\zeta}{2} \left( \frac{a}{b} + \frac{b}{a} \right) \right] \overline{(\mathbf{M} \times \mathbf{H})}_z. \quad (\text{A7})$$

Similarly we analyze the second term on the rhs of (A3) in the coordinate system  $\Sigma''$ , rotating with the angular velocity  $\boldsymbol{\Omega}$  of the drop with respect to the laboratory frame  $\Sigma$ . This gives rise to

$$-4\pi \overline{M_i \frac{d(n_{ik} M_k)}{dt}} = -4\pi \overline{M_i \frac{d'(n_{ik} M_k)}{dt}} + 4\pi \boldsymbol{\Omega} \cdot \overline{(\mathbf{M} \times \mathbf{nM})}. \quad (\text{A8})$$

In  $\Sigma''$  the shape of the drop is at rest and the demagnetizing tensor is hence constant. Choosing  $\Sigma''$  (as in the main text) such that  $n_{ik}$  is diagonal, we have

$$M_i \frac{d'(n_{ik} M_k)}{dt} = n_1 M_x \frac{d' M_x}{dt} + n_2 M_y \frac{d' M_y}{dt}, \quad (\text{A9})$$

and being a total time derivative, this expression will be identically zero after performing the time average. The first term on the rhs of (A8) therefore vanishes. Using again (14), we realize that

$$4\pi \overline{\mathbf{M} \times \mathbf{nM}} = \frac{\mathbf{L}^m}{V} - \overline{\mathbf{M} \times \mathbf{H}}, \quad (\text{A10})$$

where we have used the definition (63) of the magnetic torque  $\mathbf{L}^m$ . We hence obtain

$$-4\pi M_i \frac{d(n_{ik} M_k)}{dt} = \frac{\Omega L_z^m}{V} - \Omega \overline{(\mathbf{M} \times \mathbf{H})}_z, \quad (\text{A11})$$

and using this equation and (A7) in (A3) we get the energy dissipation balance (A1) in the form

$$W_1 + W_2 = \frac{\zeta V}{2} \left( \frac{a}{b} + \frac{b}{a} \right) \overline{(\mathbf{M} \times \mathbf{H})}_z + \Omega L_z^m. \quad (\text{A12})$$

To proceed we have to compute the viscous dissipation rates  $W_1$  and  $W_2$  inside and outside the drop. This is most conveniently done in the coordinate system  $\Sigma''$ . The energy dissipated inside the drop is then given by [29]

$$W_1 = \frac{\eta^{(i)}}{2} \int_V dV \left( \frac{\partial v_i^{(i)}}{\partial x_k} + \frac{\partial v_k^{(i)}}{\partial x_i} \right)^2. \quad (\text{A13})$$

Using the equation of motion (3), the volume integral can be reduced to a surface integral in the standard way [29] and we get

$$W_1 = \int_{\partial V} dS v_i^{(i)} (\sigma'_{ik}{}^{(i)} - p^{(i)} \delta_{ik}) \nu_k, \quad (\text{A14})$$

where  $\nu$  denotes the surface normal pointing into the surrounding liquid. In  $\Sigma''$  the normal component of the internal velocity is zero, and in view of (57) we find that  $W_1$  can be expressed solely in terms of the viscous stress tensor as

$$W_1 = \int_{\partial V} dS v_i^{(i)} \sigma'_{ik}{}^{(i)} \nu_k. \quad (\text{A15})$$

Similarly we can express the dissipation rate in the external fluid by two surface integrals, one over the surface of the drop and one over the surface  $\mathcal{S}$  of a large sphere with radius  $\mathcal{R} \gg a$ . This gives rise to

$$W_2 = \int_{\mathcal{S}} dS v_i^{(e)} (\sigma'_{ik}{}^{(e)} - p^{(e)} \delta_{ik}) \nu_k - \int_{\partial V} v_i^{(e)} \sigma'_{ik}{}^{(e)} \nu_k. \quad (\text{A16})$$

To calculate the first integral we need the behaviour of  $\mathbf{v}^{(e)}$  at large distances from the drop. From (44) and (48) and using the asymptotic properties of Jeffery's solution [19] for  $r = \sqrt{x^2 + y^2 + z^2} \rightarrow \infty$  we get to leading order

$$v_x^{(e)} = \Omega y - C \frac{x^2 y}{r^5} - D \frac{y}{3r^3}, \quad (\text{A17})$$

$$v_y^{(e)} = -\Omega x - C \frac{x y^2}{r^5} + D \frac{x}{3r^3}, \quad (\text{A18})$$

$$v_z^{(e)} = -C \frac{x y z}{r^5}, \quad (\text{A19})$$

$$p^{(e)} = -2\eta^{(e)} C \frac{x y}{r^5}, \quad (\text{A20})$$

where we introduced the abbreviations

$$C = \frac{\mathcal{R}^3 (A_{12} + A_{21})}{2}, \quad (\text{A21})$$

$$D = \frac{\mathcal{R}^3 (A_{12} - A_{21})}{2}. \quad (\text{A22})$$

Using these results we get for the first integral in (A16) in the limit  $\mathcal{R} \rightarrow \infty$

$$\begin{aligned} \lim_{\mathcal{R} \rightarrow \infty} \int_{\mathcal{S}} dS v_i^{(e)} (\sigma'_{ik}{}^{(e)} - p^{(e)} \delta_{ik}) \nu_k \\ = \Omega V \eta^{(e)} (A_{12} - A_{21}). \end{aligned} \quad (\text{A23})$$

From the comparison with (58) we see that this expression is equal to  $-\Omega L_z^v$ , which in turn equals  $\Omega L_z^m$ , i.e. the last term in (A12). Therefore we have transformed the energy dissipation balance (A1) into the relation

$$\begin{aligned} \int_{\partial V} dS (v_i^{(i)} \sigma'_{ik}{}^{(i)} - v_i^{(e)} \sigma'_{ik}{}^{(e)}) \nu_k \\ = \frac{\zeta V}{2} \left( \frac{a}{b} + \frac{b}{a} \right) \overline{(\mathbf{M} \times \mathbf{H})}_z, \end{aligned} \quad (\text{A24})$$

which observing (68) is identical with (7).

#### Acknowledgments

This work was supported by Deutsche Forschungsgemeinschaft under grant FOR 301/2-1.

- [1] S. Chandrasekhar, *Ellipsoidal Figures of Equilibrium*, Dover, New York 1987.
- [2] N. Bohr and J. A. Wheeler, *Phys. Rev.* **56**, 426 (1939).
- [3] X.-P. Huang, J. J. Bollinger, T. B. Mitchell, and W. M. Itano, *Phys. Rev. Lett.* **80**, 73 (1998).

- [4] S. R. Keller and R. Skalak, *J. Fluid Mech.* **120**, 27 (1982).
- [5] K. Ohsaka and E. H. Trinh, *Phys. Rev. Lett.* **84**, 1700 (2000).

- [6] T.G. Wang, E.H. Trinh, A.P. Croonquist, and D.D. Elleman, *Phys. Rev. Lett.* **56**, 452 (1986).
- [7] J.-C. Bacri, A. Cebers, and R. Perzynski, *Phys. Rev. Lett.* **72**, 2705 (1994).
- [8] Yu. K. Bratukhin, A. V. Lebedev, and A. F. Pshenichnikov, *Fluid Dynamics* **35**, 17 (2000).
- [9] K.I. Morozov, A. Engel, A. V. Lebedev, *Europhys. Lett.* **58**, 229 (2002).
- [10] R.E. Rosensweig, *Ferrohydrodynamics*, Cambridge University Press, Cambridge 1985.
- [11] A. V. Lebedev, A. Engel, and K.I. Morozov, *New J. Phys.* **5**, 57 (2003).
- [12] J.-C. Bacri and D. Salin, *J. Phys. (France)* **43**, L649 (1982).
- [13] A. V. Lebedev and K.I. Morozov, *JETP Lett.* **65**, 160 (1997).
- [14] K.I. Morozov, *JETP* **85**, 728 (1997).
- [15] O. Sandre, J. Browaeys, R. Perzynski, J.-C. Bacri, V. Cabuil, and R. E. Rosensweig, *Phys. Rev. E* **59**, 1736 (1999).
- [16] M. D. Cowley and R. E. Rosensweig, *J. Fluid. Mech.* **30**, 671 (1967).
- [17] E. Janiaud, F. Elias, J.-C. Bacri, V. Cabuil, and R. Perzynski, *Magneto hydrodynamics* **36**, 365 (2000).
- [18] A. Cebers and S. Lacis, *Brazil. J. Phys.* **25**, 101 (1995).
- [19] G. B. Jeffrey, *Proc. R. Soc. London, Ser. A* **102**, 161 (1922).
- [20] M. I. Shliomis, *Sov. Phys. Usp.* **17**, 153 (1974).
- [21] L. D. Landau and E. M. Lifshitz, *Electrodynamics of Continuous Media*, 2nd ed., Pergamon, New York 1984.
- [22] A. F. Pshenichnikov, *Fluid Dynamics* **31**, 14 (1996).
- [23] M. Abramowitz and I. Stegun (eds.) *Handbook of Mathematical Functions*, National Bureau of Standards, Washington D.C. 1964.
- [24] K.I. Morozov and A. V. Lebedev, *JETP* **91**, 1029 (2000).
- [25] M. A. Martsenyuk, Y. L. Raikher, and M. I. Shliomis, *Sov. Phys.-JETP* **38**, 413 (1974).
- [26] Y. L. Raikher and M. I. Shliomis, *Adv. Chem. Phys.* **87**, 595 (1994).
- [27] H. W. Müller and M. Liu, *Phys. Rev.* **E64**, 061405 (2001).
- [28] R. Roscoe, *J. Fluid. Mech.* **28**, 273 (1967).
- [29] L. D. Landau and E. M. Lifshitz, *Fluid Mechanics*, 2nd ed., Pergamon, New York 1987.